Compartmental Modeling of Iodine-123-Iodobenzofuran Binding to Dopamine D2 Receptors in Healthy Subjects

Marc Laruelle, Chris van Dyck, Anissa Abi-Dargham, Yolanda Zea-Ponce, Sami S. Zoghbi, Dennis S. Charney, Ronald M. Baldwin, Paul B. Hoffer, Hank F. Kung and Robert B. Innis

Departments of Psychiatry and Diagnostic Radiology, Yale University School of Medicine, New Haven, and West Haven Veterans Affairs Medical Center, West Haven, Connecticut; and Division of Nuclear Medicine, Department of Radiology, University of Pennsylvania, Philadelphia, Pennsylvania

Iodine-123-labeled iodobenzofuran ([^{123}I]IBF) is a potent dopamine D2 antagonist that provides good visualization of D2 receptors in primates. **Methods:** The feasibility of measuring dopamine D2 binding potential with [^{123}I]IBF in humans was evaluated in eight healthy subjects. Following [^{123}I]IBF injection (6 mCi), scans were acquired every 10 min for 160 min with the brain-dedicated CERASPECT camera. Arterial activities were obtained at various intervals and corrected for the presence of metabolites by extraction followed by reverse-phase high-performance liquid chromatography. **Results:** Reconstructed images exhibited adequate basal ganglia-to-occipital ratios (from 1.96 ± 0.34 at 30 min to 3.54 ± 0.71 at 150 min, mean ± s.d.). Time-activity curves demonstrated reversibility, with peak basal ganglia uptake at 50 ± 25 min. Regional time-activity curves were analyzed with kinetic three-compartment modeling and graphic analysis. In all subjects, D2 binding potential values, as derived by both methods, were in excellent agreement (mean ± s.d. D2 binding potential = 129 ± 51). An empiric count ratio method that does not require measurement of arterial tracer concentrations was evaluated and found to be in reasonable agreement with the model-derived binding potential. **Conclusion:** Iodine-131-IBF is a suitable ligand for quantitative studies of D2 receptor density with SPECT in humans.

Key Words: SPECT; dopamine D2 receptors; iodine-123-IBF; kinetic analysis

J Nucl Med 1994; 35:743–754

Over the last few years, several iodinated substituted benzamides suitable for imaging dopamine D2 receptors with SPECT have been proposed. The first compound of this class to be introduced, [^{123}I]IBZM (K_D = 0.43 n*M*), (*1*) has been used in several clinical studies of conditions, such as Parkinson's disease, Huntington's disease, progressive supranuclear palsy and schizophrenia (*2–6*). More recently, new iodinated benzamides have been developed as potential SPECT tracers. Ligands, such as [^{123}I]iodobenzofuran (IBF) (K_D = 0.11 n*M*), [^{123}I]NCQ 298 (K_D = 0.02 n*M*) and [^{123}I]epidipride (K_D = 0.02 n*M*), exhibited higher affinities for D2 receptors and produced higher striatal-to-cerebellar ratios than did [^{123}I]IBZM (*7–10*).

The basal ganglia-to-cerebellum ratio is typically used to analyze [^{123}I]IBZM SPECT data, yet this empiric outcome measure might be affected by between-subject differences in factors not related to the receptors, such as peripheral clearance, nonspecific binding to plasma proteins or cerebral tissue and regional cerebral blood flow. Hence, these empiric measures need to be evaluated with model-based methods that characterize the regional response to the arterial input function and provide quantitative estimations of receptor parameters (*11–14*). For studies performed at tracer doses (high specific activity and negligible receptor occupancy), the receptor parameter of interest is the binding potential (BP), equal to the product of the density and affinity of the receptors (B_{max}/K_D, *14*).

Model-based methods are technically demanding, and their accuracy depends on the validity of the model and on the precision of the measurements needed for their implementation. For example, errors in plasma measurements or variations in the cross calibration between plasma and brain counting devices may produce biases in the estimation of the receptor parameters. Thus, the more explicit models are not always the most desirable from the point of view of error propagation.

The aim of the present study was to evaluate the feasibility of using model-based methods to derive the dopamine D2 BP with [^{123}I]IBF and SPECT in human subjects. Because these methods require short acquisition times to measure regional time-activity curves with adequate temporal resolution, high target-to-background ratios are needed. High contrasts are obtained with tracers that exhibit both high affinity and low lipophilicity (*10*). However,

Received Aug. 30, 1993; revision accepted Jan. 26, 1994.
For correspondence or reprints contact: Marc Laruelle, MD, Department of Psychiatry, Yale School of Medicine, West Haven VA Medical Center/116A2, West Haven, CT 06516.

because measurement of BP requires equilibrium (i.e., peak of specific uptake, *15*) to occur within the time frame of the experiment (*13*), the ligand must exhibit rapid in vivo reversibility, which is better achieved by ligands with moderate affinity and high lipophilicity. In baboons, [^{123}I]IBF was found to provide an adequate balance between these conflicting requirements (*15,16*). The [^{123}I]IBF achieved striatal-to-occipital ratios of 2:2.5 at striatal peak uptake (20–40 min) and of 6:8 at 150 min postinjection. The striatal peak was followed by a rapid washout (about 30% of striatal activity per hour). Thus, [^{123}I]IBF was selected as a potential candidate for measurement of D2 BP in human studies.

In this study, three equilibrium distribution volumes of the receptor compartment were used as outcome measures: the equilibrium distribution volume of the receptor compartment relative to the arterial free tracer (V_3, equal to the BP), relative to the arterial total tracer (V_3') and relative to the nondisplaceable compartment ($V(_3)$. Two model-based methods, referred to as kinetic and graphic analyses, were used to derive these outcome measures. The kinetic analysis derives the BP from the ratio of the kinetic rate constants describing the transfer of the tracer between the plasma, nondisplaceable and specific compartments (*14,17–19*). The graphic method of Logan et al. (*20*) allows direct calculation of BP for reversible ligands (i.e., without prior derivation of the rate constants). Results of both kinetic and graphic methods were compared with results of an empiric method based on the basal ganglia-to-occipital activity ratio measured over 40 min (80–120 min postinjection).

METHODS

Radiolabeling

Labeling of [^{123}I]IBF was performed as previously described (*15,21*). Briefly, to a 1-ml vial containing 50 μg of tributylstannyl precursor in 50 μl ethanol were added, in the following order, sufficient 0.5 *M* H_3PO_4 to adjust the pH to 3 (about 20% of the volume of [^{123}I]NaI), 100 to 500 μl (20–30 mCi) [^{123}I]NaI and 50 μl of 1.3% peracetic acid. After 20 to 30 min at room temperature, 100 μl (100 μg) of aqueous $NaHSO_3$ and 1 ml of saturated $NaHCO_3$ solution were added, and the reaction mixture was extracted with 3 × 1 ml of ethyl acetate. The solvent was evaporated to dryness on a rotary evaporator with a stream of nitrogen or argon, the residue was dissolved in 50 to 100 μl of methanol, mixed with an equal volume of water and separated by high-performance liquid chromatography (HPLC) using the following system: 8-mm 4-μ Novapak C18 cartridge with radial compression module (RCM 8 × 10, Waters Associates, Milford, MA) and methanol-to-water-to-triethylomine (75:25:0.2), 0.7 ml/min. The fraction-containing product was collected in a 25-ml pear-shaped flask containing 100 μl (100 μg) of aqueous L-ascorbic acid and evaporated to dryness. Iodine-123-IBF was obtained in an average labeling yield of 75.3% ± 6.0% (with this and subsequent values expressed as mean ± s.d., unless otherwise specified) and radiochemical purity of 95.8% ± 2.5%. The specific activity was too great to measure with the sensitivity of the ultraviolet detector on the HPLC and was estimated to be at least 5000 Ci/mmole. Sterility and apyrogenicity were confirmed by compendial tests (*22*).

Healthy Subjects

Eight healthy subjects (four women and four men, age range 27 ± 5 yr, weight range 69 ± 15 kg) were recruited for these studies. Inclusion criteria were absence of current medical conditions and absence of history of neuropsychiatric illness. Physical examination, electrocardiography and routine biological tests were performed in the screening procedure. All subjects gave written informed consent. Protocols were approved by the local Human Investigation Committee. The subjects received 0.6 g of potassium iodide (supersaturated potassium iodide solution) in the 24 hr prior to imaging.

Data Acquisition

SPECT data were acquired with the multislice brain-dedicated CERASPECT camera (Digital Scintigraphics, Walthan, MA; *23*) with a transaxial and axial resolution of 7.7 and 5.9 mm full width at half maximum, respectively (*24*). Before each experiment, an ^{123}I point source (117 ± 33 μCi) was positioned in the center of the field of view for sensitivity calibration. Mean point source sensitivity was 6224 ± 804 cps/mCi. Four fiducial markers filled with 10 μCi of [^{99m}Tc]NaO_4 were glued on each side of the subject's head at the level of the canthomeatal line. These fiducial markers were used to control for adequate positioning of the subject's head in the gantry before tracer injection and to identify the canthomeatal plane during image analysis. A catheter was inserted in the radial artery for blood sampling.

Iodine-123-IBF (5.9 ± 0.02 mCi) was injected as a single bolus over a 30-sec period. Scans were acquired continuously until 160 min postinjection. Acquisition times were 5 min for the first two scans and 10 min thereafter. Arterial samples were obtained every 10 sec for the first 2 min with a peristaltic pump (Harvard 2501-001, South Natick, MA). Subsequent samples were obtained manually at 3, 4, 6, 8, 10, 12, 16, 20 and 30 min and every 15 min until 200 min.

Arterial Plasma Analysis

Arterial samples were analyzed as previously described (*15,25*). Extraction (ethyl acetate) was followed by reverse-phase HPLC to measure the metabolite-corrected total plasma activity ($C_a(t)$, in μCi/ml). Plasma protein binding was measured in vitro by ultracentrifugation through four Centrifree membrane filters (Amicon, Beverly, MA), the parent compound free fraction being calculated as the ratio of the filtrate concentration to the total concentration (average within-run s.e.m. was 7% ± 4% of the mean). The equilibration with plasma protein was assumed to be rapid compared with the other processes measured in these experiments so that the free fraction of plasma parent compound measured by ultracentrifugation (f_1 = free parent/$C_a(t)$, *14*) was assumed to be constant over time.

The measured metabolite-corrected plasma activities were fit to a sum of three exponentials

$$C_a(t) = C_0 \sum_{i=1}^{3} a_i e^{-\lambda_i t} \qquad \text{Eq. 1}$$

where C_0 (in μCi/liter) is the peak plasma concentration, a_i is the relative zero-time intercept of each exponential and λ_i is the elimination rate constant associated with each exponential (in reciprocal minutes). The terminal half-life of the tracer in the plasma was calculated as ln (2)/λ_3 (in minutes). The initial distribution

volume of the tracer, V_{bol} (in liters), was calculated as the ratio of the injected dose, D (in millicuries) to C_0 and expressed as a percent of body weight. The plasma clearance (C_L, in liters per hour) was calculated as

$$C_L = 60 \frac{D}{C_0 \sum_{i=1}^{3} a_i/\lambda_i}. \quad \text{Eq. 2}$$

SPECT Data Analysis

Images were reconstructed from photopeak counts (159 ± 16 keV) with a Butterworth filter (cutoff = 1 cm, power factor = 10) and displayed on a 64 × 64 × 32 matrix (pixel size = 3.3 × 3.3 mm, slice thickness = 3.3 mm and voxel volume = 36.7 mm^3). Attenuation correction was performed by assuming uniform attenuation equal to that of water (attenuation coefficient $\mu = 0.15$ cm^2/g) within an ellipse drawn around the skull as identified by the markers. Images were reoriented in the three dimensions so that the canthomeatal plane, as identified by the four fiducial markers, corresponded to the transaxial plane of the dataset. The four slices corresponding to the highest basal ganglia activities were then summed. Three regions of interest were positioned on this summed image at the level of the right and left basal ganglia (852 mm^2 each) and the occipital pole (3963 mm^2). The occipital region was used as the region of reference because its contains only negligible concentration of D2 receptors (*26*). In baboons, intravenous injection of a receptor-saturating dose of unlabeled raclopride (1 mg/kg) did not produce any displacement of activity in the occipital pole, but it reduced the striatal activity to the level observed in the occipital pole, which was chosen as the region of reference because this cerebellum is difficult to localize properly without CT or MRI coregistration.

Average counts per minute per pixel activities were measured, decay-corrected for the time of injection and expressed in microcuries per cubic centimeter by using a calibration factor derived from a ^{123}I distributed source acquired using the same protocol. Activities from right and left basal ganglia were averaged. Deadtime losses were estimated from the acquisition total counts over the entire energy spectrum (35–250 keV) and were negligible in these studies. No attempts were made to correct for partial volume effects or for the scatter fraction of the photopeak window.

Kinetic Method. A three-compartment model (Fig. 1) was used to analyze time-activity curves in the basal ganglia. The model included the capillary plasma compartment (C_1), the intracerebral free and nonspecifically bound compartment (nondisplaceable compartment, C_2) and the specifically bound compartment (C_3). In the nondisplaceable compartment, the nonspecifically bound compartment was assumed to be at equilibrium at all times. A two-compartment model was used in the occipital region, a region with negligible D2 receptor density (*26*).

The equilibrium distribution volume of a compartment i (V_i, in ml/g) was defined as the ratio of the tracer concentration in this compartment-to-the free arterial concentration at equilibrium (*27*),

$$V_i = \frac{C_i}{f_1 C_a}. \quad \text{Eq. 3}$$

V_2 and V_3 were defined as the equilibrium distribution volume of the second and third compartments, respectively, with V_T being the total regional equilibrium distribution volume, equal to the sum of V_2 and V_3.

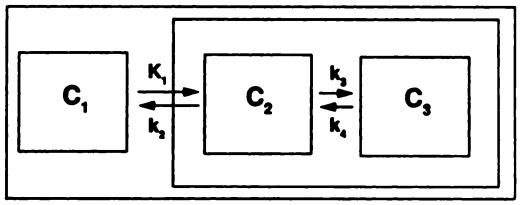

FIGURE 1. Compartment configuration used to model [^{123}I]IBF uptake kinetics; C_1 = plasma compartment; C_2 = intracerebral free and nonspecifically bound compartment (referred as nondisplaceable compartment); C_3 = specifically bound compartment; K_1 to k_4 = fractional rate constants of the transfer between compartments. For practical implementation, arterial plasma concentration (C_a) was used as input function to C_2. Free and nonspecific binding were assumed to be at equilibrium at all times in plasma and brain.

Similarly, V_2', V_3' and V_T' (in ml/g) were defined as the equilibrium distribution volumes relative to the total (i.e., free plus protein bound) arterial tracer

$$V_i' = \frac{C_i}{C_a}. \quad \text{Eq. 4}$$

V_3'' (unitless) was defined as the equilibrium distribution volume of the receptor compartment relative to the equilibrium distribution volume of the nondisplaceable compartment

$$V_3'' = \frac{V_3}{V_2}. \quad \text{Eq. 5}$$

The tracer concentration over time in each compartment was given by

$$\frac{dC_2(t)}{dt} = K_1 C_a(t) - k_2 C_2(t) - k_3 C_2(t) + k_4 C_3(t), \quad \text{Eq. 6}$$

$$\frac{dC_3(t)}{dt} = k_3 C_2(t) - k_4 C_3(t). \quad \text{Eq. 7}$$

The kinetic parameters were defined as follows

$$K_1 = FE = F(1 - e^{-PS/F}) \quad \text{(in ml/g/min)}, \quad \text{Eq. 8}$$

$$k_2 = K_1/V_2 f_1 \quad \text{(in reciprocal minutes)}, \quad \text{Eq. 9}$$

$$k_3 = k_{on} B'_{max}/V_2 \quad \text{(in reciprocal minutes)}, \quad \text{Eq. 10}$$

$$k_4 = k_{off} \quad \text{(in reciprocal minutes)}, \quad \text{Eq. 11}$$

where F is the regional blood flow (in ml/g/min), E is the unidirectional extraction fraction, PS is the permeability surface area product of the tracer (in ml/g/min), k_{on} is the bimolecular ligand-receptor association rate constant ($min^{-1} \cdot mM^{-1}$), B'_{max} is the concentration of receptors available for binding (equal to B_{max} because all experiments were performed at tracer doses) and k_{off} is the receptor's dissociation rate constant (min^{-1}).

Kinetic analysis derived the equilibrium distribution volume from the ratio of the rate constants (Table 1). The relationship between V_2 and the kinetic parameters K_1 and k_2 (Equation 9) was derived from Equation 6 by setting k_3, k_4 and the derivative to zero. Similarly, setting the derivatives in Equation 7 to zero and substituting with Equations 3 and 9 gives

$$V_3 = \frac{K_1 k_3}{k_2 k_4 f_1}. \quad \text{Eq. 12}$$

TABLE 1
Outcome Measures

Outcome measure	Relationship to rates constants	Relationship to BP	Factors controlled by outcome measure (yes/no)*			
			Plasma clearance	Binding to plasma protein	Intracerebral nonspecific binding	Regional cerebral blood flow
V_3	$= \frac{K_1k_3}{k_2k_4f_1}$	$= BP$	Y	Y	Y	Y
V_3'	$= \frac{K_1k_3}{k_2k_4}$	$= BPf_1$	Y	N	Y	Y
V_3''	$= \frac{k_3}{k_4}$	$= \frac{BP}{V_2}$	Y	Y	N	Y
$\frac{Bg - Occ}{Occ}$	—	—	N	Y	N	N

*Yes: the outcome measure is protected from potential between-subject or between-group differences in these factors. No: the outcome measure might be biased by potential between-subject or between-group differences in these factors.

V_3 = equilibrium distribution volume of the receptor compartment relative to the free arterial tracer; V_3' = equilibrium distribution volume of the receptor compartment relative to the total arterial tracer; V_3'' = equilibrium distribution volume of the receptor compartment relative to the equilibrium distribution volume of the nondisplaceable compartment (V_2); K_1 to k_4 = fractional rate constants; f_1 = free fraction in plasma; BP = binding potential (B_{max}/K_D); Bg and Occ = average basal ganglia and occipital activities (this empiric outcome measure is equal to V3" only at peak time of (Bg − Occ).)

V_T is given by the sum of V_2 and V_3 (Equations 9 and 12)

$$V_T = \frac{K_1(1 + k_3/k_4)}{k_2f_1}. \qquad \text{Eq. 13}$$

Substituting in Equation 12 the terms K_1/k_2f_1, k_3 and k_4 with Equations 9, 10 and 11, respectively, and recalling that K_D is equal k_{off}/k_{on}, established the equivalence between V_3 and BP. The relationships between V_3', V_3'', the rate constants and the BP followed a similar derivation and are given in Table 1.

The contribution of the activity in the blood vessels to the total regional activity was estimated using the total plasma activity integrated over the acquisition time and a mean blood volume equal to 5% of the regional volume (*14*). This contribution was found to be negligible (<0.5%). The occipital equilibrium distribution volume was assumed to be equal to the nondisplaceable compartment in the basal ganglia (V_2). This assumption was validated in baboons in which the striatal [^{123}I]IBF equilibrium distribution volume after injection of a receptor-saturating dose of raclopride (1 mg/kg intravenous) was found to be equal to the occipital equilibrium distribution volume (*16*). Hence, the model constrained the K_1-to-k_2 ratio in the basal ganglia to the K_1-to-k_2 ratio measured in the occipital. Because this ratio is independent of the blood flow (Equations 8 and 9), the model did not assume similar blood flow in both regions.

Kinetic parameters were derived with an analytic solution. Fitted brain values were calculated by the convolution of the arterial input function and the impulse response function, which was a sum of 1 (occipital) or 2 (basal ganglia) exponentials, as previously described (*18,28,29*). Rate constants for arterial clearance and brain uptake of the tracer were estimated by nonlinear regression, using a Levenberg-Marquart least-squares minimization procedure (*30*) implemented in MATLAB (The Math Works, Inc., South Natick, MA). Preliminary runs established that the minimization procedure was not sensitive to initial values. In all cases, the program converged before the maximum number of iterations was exceeded (set at $100 \cdot p$, with p equal to the number of parameters free to float). Metabolite-corrected fitted arterial tracer concentration values were used as the input function (*17*). Values were calculated every 10 sec for the first 2 min and every 2 min for the remainder of the experiment. Preliminary exploration of the model showed that using denser input functions did not change the results of the optimization procedure.

The standard errors of the parameters were given by the diagonal of the covariance matrix (*31*) and expressed as the percent of the parameters (coefficient of variation). This is a measure of the identifiability of the parameters by the regression process. The parameter identifiability measure should not be confused with the standard deviation of the parameter in the sampled population.

Graphic Method. Regional time activity curves were graphically analyzed according to the equation

$$\frac{\int_0^0 C_{ROI}(t)dt}{C_{ROI}(t)} = a\frac{\int_0^t f_1C_a(t)dt}{C_{ROI}(t)} + b, \qquad \text{Eq. 14}$$

where the value of the slope a and the intercept b are obtained by linear regression and ROI indicates region of interest. This method allows the determination of the regional V_T of reversible ligands as the slope of the regression line without assuming a particular compartmental configuration (*20*). Integrations were performed numerically using a recursive Simpson's rule. Assuming, as in the kinetic analysis, the equivalence between the nondisplaceable basal ganglia and occipital equilibrium distribution volumes, BP was calculated as the difference between the slope of the regression lines in the basal ganglia and occipital regions.

Although derivations of the kinetic parameters are not needed for an estimation of BP, their values can be computed using the intercept of the regression lines by solving the following system of equations (*20*):

$$K_1 = a_{occ}k_2, \qquad \text{Eq. 16}$$

$$k_2 = -1/b_{occ}, \qquad \text{Eq. 17}$$

$$k_3 = a_{bg}k_4, \qquad \text{Eq. 18}$$

$$k_4 = -\frac{(k_2/(1 + V_3) + 1/b_{bg})}{(1 + V_3)}, \qquad \text{Eq. 19}$$

where a and b are slopes and intercepts of the occipital (occ) and basal ganglia (bg) regression lines.

Empiric Method. The ratio of the specific (basal ganglia minus occipital) to nonspecific (occipital) activity measured from 80 to 120 min (four acquisitions) was calculated and compared with V_3''. Providing that the specific binding is at equilibrium, these two outcome measures should give similar results. This period was chosen after completion of the studies because it was centered around the average peak time of the specific binding, empirically calculated as the difference between the basal ganglial and occipital activity.

RESULTS

Peripheral Metabolism and Clearance

The radiopharmaceutical [^{123}I]IBF was metabolized into two operationally defined fractions (Fig. 2A): a polar fraction (nonextractable in ethyl acetate) and a lipophilic fraction (extractable in ethyl acetate). HPLC analysis revealed that the extractable fraction was composed of the parent compound and two distinct metabolites that eluted before the parent compound (Fig. 2B). The relative contribution of the polar fraction increased rapidly to about 20% of total activity within 20 to 40 min and then remained relatively stable. By contrast, the lipophilic metabolite fraction steadily increased for the first 60 min postinjection and then stabilized at 60%–70% of total activity. Hence, the parent compound fraction decreased during the first hour to 10%–20% of the total activity. The polar, lipophilic and parent fractions represented 18% ± 5%, 58% ± 9% and 23% ± 11% of the total activity at 60 min and 26% ± 13%, 70% ± 25% and 17% ± 9% at 120 min.

Pharmacokinetic parameters of the plasma clearance of the parent compound were estimated by three-exponential fit (Equations 1 and 2, Table 2, Fig. 3). The mean V_{bol} was 7.4% ± 3.2% of body weight, a value close to the estimated blood volume (8%; *32*). Both C_L (41 ± 21 liters/hr) and terminal half-life (115 ± 100 min) values showed large variation between subjects. The mean f_1 was 0.05% ± 0.02%, indicating that 95% of the parent compound was bound to plasma proteins. The value of f_1 ranged from 0.024% to 0.065%. Between-subject differences in f_1 were significant compared with the assay reproducibility (repeated-measures analysis of variance [ANOVA]; between-subjects, n = 8, p = 0.001; within-subjects, n = 4, p = 0.69).

Occipital Region

Occipital activity displayed an early peak (12 ± 6 min) and a rapid washout. Occipital time-activity curves were analyzed with kinetic and graphic methods (Table 3, Figs. 4 and 5).

Kinetic Analysis. The mean K_1 and k_2 were 0.086 ± 0.0161 ml · g^{-1} · min^{-1} and 0.036 ± 0.004 min^{-1}. Both parameters were well identified, with a mean identification of 6.3% ± 1.6% and 7.6% ± 2.0%, respectively. V_2 was 54 ± 18 ml/g with an identifiability of 3.6% ± 1.4%. V_2' was 2.44 ± 0.52 ml/g.

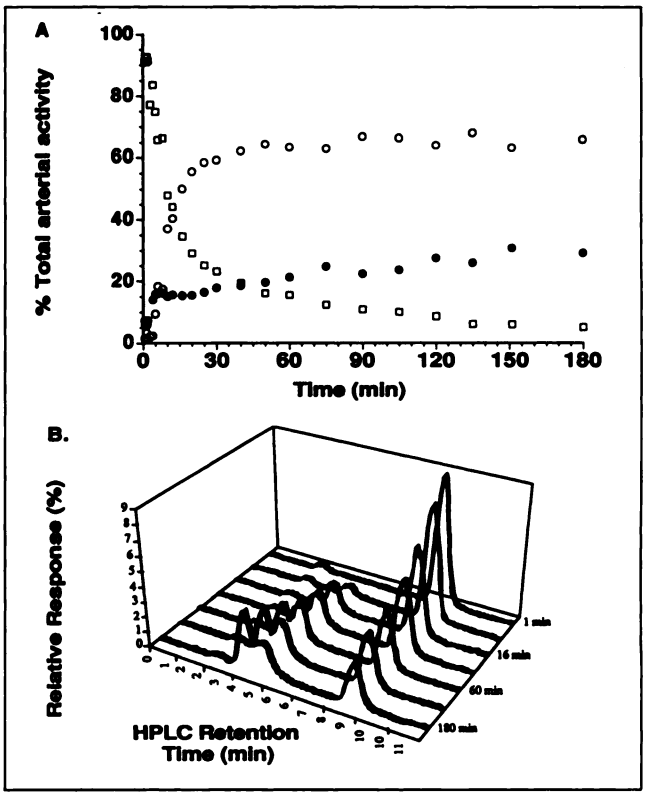

FIGURE 2. Peripheral metabolism of [^{123}I]IBF after injection of 5.6 mCi in a 33-yr-old female (Subject 4). (A) Iodine-123-IBF underwent extensive metabolism into two classes of metabolites, a polar fraction (closed circles) not extractable by ethyl acetate, and a lipophilic fraction (open circles) extractable by ethyl acetate. The parent compound (open squares) was separated from the lipophilic metabolites by reverse-phase HPLC. The y-axis represents the respective contribution of each class to the total arterial activity. The contribution of the parent compound decreased rapidly to about 20% and 10% at 60 and 120 min, respectively. (B) Relative distribution of lipophilic plasma components at selected times as determined by reverse-phase HPLC, shown as relative response of the radioactive detector normalized so that the sum of the area under the peak equals 100%. The parent compound eluted at retention time (t_R) 8.9 min. Two lipohilic metabolites were detected at t_R 4.3 and 5.1 min.

Graphic Analysis. Because the relationship appeared to be linear over the entire duration of the studies (Fig. 5B), every point was included in the regression. The values of V_2 as derived by graphic analysis (55 ± 20 ml/g) were virtually identical to V_2 values estimated by kinetic analysis (54 ± 18 ml/g). Graphically derived values of K_1 and k_2 were also very close to the kinetically derived values (Table 3).

Basal Ganglia

Basal ganglial activities peaked at 50 ± 25 min. In subjects with slow peripheral clearance, the basal ganglial activity exhibited a prolonged plateau. In subjects with fast clearance, the basal ganglial activity showed an earlier and sharper peak followed by a faster washout. The ratio of basal ganglial-to-occipital activities were 1.96 ± 0.34,

TABLE 2
Demographic Data and Plasma Analyses

Study no.	Sex	Age (yr)	Weight (kg)	[^{123}I]IBF dose (mCi)	V_{bol} (% body weight)	C_L (liter/hr)	Terminal half-life (min^{-1})	f_1
1	F	23	73	6.1	5.4	39.0	104	0.070
2	F	24	48	5.6	14.5	20.5	349	0.048
3	F	24	77	6.0	7.9	63.9	68	0.054
4	F	33	53	5.6	7.2	53.4	47	0.065
5	M	22	57	6.0	7.7	74.0	35	0.024
6	M	23	89	6.1	6.4	20.7	136	0.064
7	M	28	80	5.8	6.2	41.8	74	0.046
8	M	43	75	6.0	3.6	15.1	110	0.027
Mean ± s.d.		28 ± 7	69 ± 15	5.9 ± 0.2	7.4 ± 3.2	41.1 ± 21	115 ± 100	0.050 ± 0.017

V_{bol} = initial arterial plasma volume of distribution, expressed as percent body weight; C_L = arterial plasma clearance of the parent compound, as calculated by three-exponential fit; terminal half-life = longest half-life of the arterial plasma clearance; f_1 = free fraction of [^{123}I]IBF in arterial plasma, measured by in vitro ultrafiltration; [^{123}I]IBF = iodine-123-labeled iodobenzofuran.

2.64 ± 0.42 and 3.54 ± 0.71 at 30, 60 and 150 min, respectively (Fig. 4). Basal ganglia curves were analyzed with kinetic, graphic and empiric methods (Tables 4 and 5, Fig. 5).

Kinetic Analysis. Basal ganglial time-activity curves were fit to a three-compartment model with the K_1-to-k_2 ratio constrained to the occipital V'_2 value. The mean value of K_1 in the basal ganglia (0.123 ± 0.03 ml g^{-1} min^{-1}) was significantly higher than in the occipital (0.086 ± 0.0161 ml g^{-1} min^{-1}; repeated-measures ANOVA; for subjects, p = 0.03; for regions, p = 0.02), but the identifiability was comparable (6.1% ± 2.1%). The mean value of k_3 and k_4 were 0.087 ± 0.049 and 0.035 ± 0.020 min^{-1}. As opposed to K_1, individual values of k_3 and k_4 were poorly identified (34% ± 25% and 38% ± 24% for k_3 and k_4, respectively).

The mean V_3 (= BP) value was 129 ± 51 ml/g and was well identified (5.6% ± 4%). Thus, the k_3-to-k_4 ratio was better identified than the individual values of k_3 and k_4. The mean V'_3 (= BPf_1) was 6.0 ± 1.8 ml/g, and the mean V''_3 (= BP/V_2) was 2.51 ± 0.73. No linear relationship was found between V_3 and V'_3 (r^2 = 0.07, p = 0.50). The source of variance in V_3 was investigated by multiple regression with f_1 and V'_3 as factors. The f_1 factor was significant (p = 0.043) but not the V'_3 factor (p = 0.16). Thus, the variance in binding potential between subjects was the result of variance in f_1 more than in V'_3.

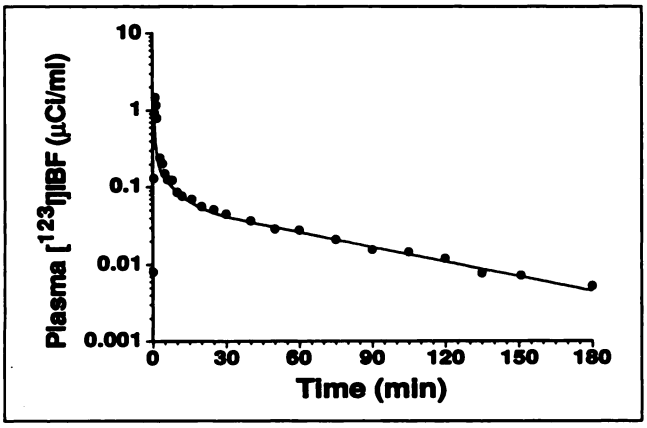

FIGURE 3. Peripheral clearance of [^{123}I]IBF after injection of 5.6 mCi in a 33-yr-old female (Subject 4). The measured total parent compound concentrations (closed circles) were fit to a sum of three exponentials (solid line) by nonlinear least-squares regression (Equation 1). Regression parameters were: initial volume of distribution, 3.7 liters; a_1, 1.15; a_2, 0.111; a_3, 0.0422; λ_1, 1.70 min^{-1}; λ_2, 0.163 min^{-1}; λ_3, 0.0146 min^{-1}; terminal half-life, 47 min and clearance, 53 liters/hr.

Graphic Analysis. All points were included in the regression. The basal ganglia V_T as estimated by the slope of the graph (184 ± 59 ml/g) was in agreement with the basal ganglia V_T, as derived by kinetic analysis (186 ± 62 ml/g). The graphic V_3 value, calculated as the difference between basal ganglia and occipital slope was 129 ± 51 ml/g, in close agreement with the kinetically derived V_3 (132 ± 51 ml/g). Individual determinations of BP by kinetic and graphic methods were in good agreement. The relationship between kinetic and graphic BP was linear with a slope (1.13) and r^2 (0.94) close to unity (p = 0.0001, Fig. 6A).

Empiric Method. For each acquisition, specific binding was estimated by the difference between basal ganglial and occipital activities. The mean peak time of the specific binding was 95 ± 32 min. Because the model predicts that the specific-to-nonspecific ratio is equal to V''_3 at the peak time of specific binding, the 80- to 120-min period was chosen as the period during which an empiric specific-to-nonspecific ratio should approximate the V''_3, as estimated by model-based methods. Over this period, the specific-to-nonspecific ratio was 2.24 ± 0.53 (Table 5), a value close to V''_3 (2.52 ± 0.73). However, linear regression between this empiric ratio and V''_3, although significant (p = 0.010), had a slope (0.60) and a correlation coefficient (0.68) far from unity (Fig. 6B). The largest discrepancy was noted in the subjects who exhibited both slow clearance and high BP. Excluding these two subjects, the slope and r^2 would have been 1.13 and 0.88, respectively.

TABLE 3
Occipital Region: Kinetic and Graphic Analyses*

Study no.	Kinetic analysis				Graphic analysis				Difference (%)
	K_1 (ml g^{-1} min^{-1})	k_2 (min^{-1})	V_2 (ml/g)	V_2' (ml/g)	K_1 (ml g^{-1} min^{-1})	k_2 (min^{-1})	V_2 (ml/g)	V_2' (ml/g)	
1	0.1158	0.0373	44.3	3.10	0.1016	0.0322	37.9	2.5	1.82
2	0.0920	0.0355	54.0	2.59	0.0947	0.0364	54.2	2.6	0.46
3	0.0893	0.0304	54.4	2.94	0.0768	0.0278	51.3	2.8	5.74
4	0.0954	0.0387	37.9	2.46	0.0835	0.0321	61.2	2.8	5.71
5	0.0703	0.0324	90.3	2.17	0.0616	0.0267	28.7	1.8	6.27
6	0.0812	0.0442	28.7	1.84	0.0758	0.0410	61.0	1.6	0.61
7	0.0880	0.0321	59.7	2.75	0.0818	0.0290	95.9	2.3	2.53
8	0.0633	0.0385	60.9	1.64	0.0594	0.0361	45.1	3.2	0.15
Mean ± s.d.	0.0869 ± 0.0161	0.0361 ± 0.0045	53.8 ± 18.5	2.44 ± 0.52	0.0794 ± 0.0146	0.0326 ± 0.0049	54.4 ± 20.1	2.5 ± 0.5	2.91 ± 2.60

*Difference between the two methods was calculated as the absolute value of the difference between kinetic V_2 and graphical V_2, expressed as the percentage of kinetic V_2.

K_1 and k_2 = fractional rate constants of the tracer transport in and out of the brain; V_2 = equilibrium distribution volume relative to free tracer in arterial plasma; V_2' = equilibrium distribution volume relative to total tracer in arterial plasma.

Simulations

To investigate relationships between empirically and kinetically derived outcome measures further, we compared the brain response with various input functions (i.e., various plasma clearances) while maintaining the parameters of the impulse response function constant. The parameters of the impulse response function were average parameters measured in this study: occipital: K_1, 0.087 ml g^{-1} min^{-1}; k_2, 0.036 min^{-1} and V_2', 2.44 ml/g and basal ganglia: K_1, 0.120 ml g^{-1} min^{-1}; k_2, 0.050 min^{-1}; k_3, 0.088 min^{-1}; k_4, 0.035 min^{-1}; V_3', 6.10 ml/g; V_T, 8.55 ml/g and V_3'', 2.49. The control input function had a clearance equal to the mean C_L (41 ± 22 liters/hr) in this population: V_{bol}, 3.8 liters; a_1, 0.83; a_2, 0.082; a_3, 0.030; λ_1, 1.69 min^{-1}; λ_2, 0.082 min^{-1} and λ_3, 0.0071 min^{-1} (corresponding to a terminal half-life of 96 min).

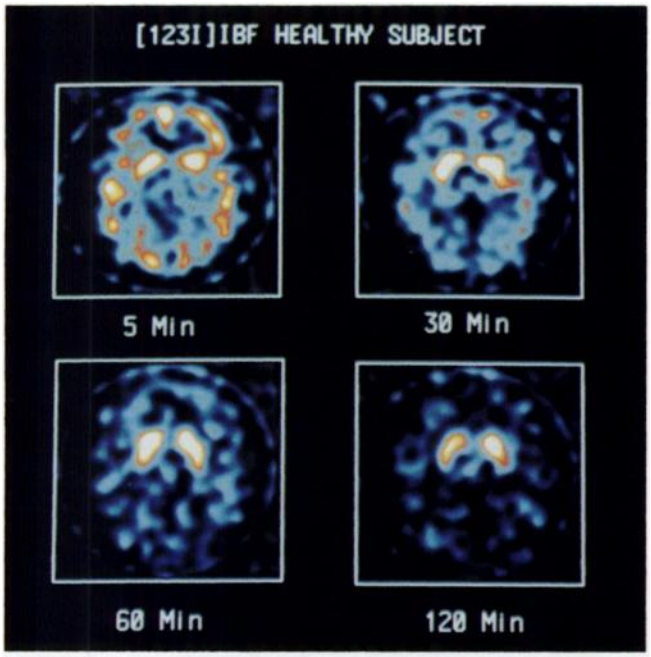

FIGURE 4. Activity distribution of [^{123}I]IBF after injection of 5.5 mCi in a 28-yr-old female (Subject 2). Acquisitions were obtained for 10 min with the CERASPECT camera at 5, 30, 60 and 120 min postinjection and reoriented so that the canthomeatal plane corresponded to the transaxial axis of the dataset. The four contiguous images, including the highest level of basal ganglial activities, were summed to generate these images. Basal ganglial-to-occipital ratios were 1.6, 2.0, 2.9 and 4.3 at 5, 30, 60 and 120 min, respectively.

The brain response to the control input function was compared with the brain responses to input functions characterized by fast or slow clearance. Fast and slow clearance input function corresponded to clearance 1 s.d. above (63 liters/hr) or 1 s.d. below (19 liters/hr) the population mean clearance and were obtained by setting λ_3 to 0.0135 and 0.0028 min^{-1}, respectively (Fig. 7A). The time of peak specific binding was 82, 96 and 125 min in the fast, control and slow clearance simulation, respectively (Fig. 7B). At the peak time, the specific-to-nonspecific ratios of the three curves were identical (2.49) and corresponded to the true value of V_3'' (2.49, Fig. 7B). When this ratio was calculated between 80 and 120 min, as in the studies presented here, the control curve yielded a ratio (2.50) similar to V_3''. However, ratios obtained from the fast and slow clearance simulations (3.11 and 2.14, respectively) resulted in over- and underestimations of the true V_3''.

DISCUSSION

These studies support the feasibility of kinetic measurement of dopamine D2 BP in humans with [^{123}I]IBF. This approach requires the measurement of the metabolite-corrected arterial input function, because marked differences were noted in the population in the rate of both peripheral metabolization and peripheral clearance.

Two model-based methods (kinetic and graphic) were used to derive the BP. Both methods used the same assumption, i.e., that the occipital equilibrium distribution

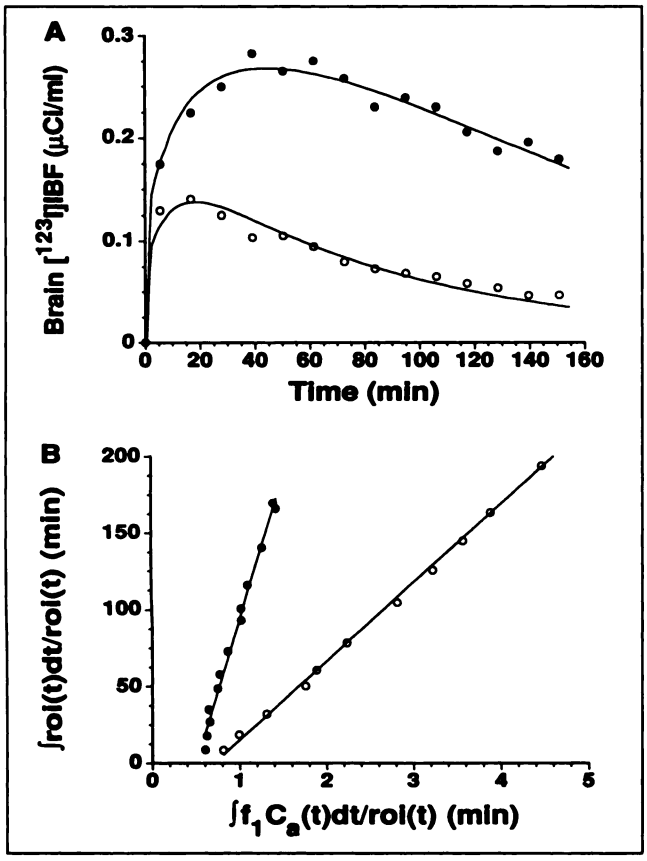

FIGURE 5. Kinetic and graphic analyses of time-activity curves in basal ganglial (closed circles) and occipital (open circles) regions following injection of 6.0 mCi [^{123}I]IBF in a 23-yr-old female (Subject 3). (A) Kinetic analysis. Measured values (circles) were fit to a two- and three-compartment model (Fig. 1) in occipital and basal ganglial regions, respectively, with basal ganglial V_2 value constrained to the value of occipital V_2. Solid lines represent the fitted values. Values of rate constants are given in Tables 3 and 4. Occipital V_2 was 54 ml/g, basal ganglia V_3 and V_T were 139 and 195 ml/g, respectively. (B) Graphic analysis. $\int_0^t C_{ROI}(t)dt/C_{ROI}(t)$ was plotted versus $\int_0^t f_1 C_a(t)dt/C_{ROI}(t)$, where $C_{ROI}(t)$ was the activity concentration in the ROI for each acquisition and $f_1C_a(t)$ was the integrated free tracer concentration during each acquisition. Because of the linear aspect of the curves, all data points were included in the linear regression: occipital lobe: $y = -36 + 51x$; basal ganglia: $y = -90 + 183x$. Occipital V_2 and basal ganglial V_T were given by the slopes (51 and 183 ml/g, respectively). Basal ganglial V_3 was calculated as 185 − 51 = 132 ml/g. Graphically and kinetically derived volumes of distribution were in excellent agreement.

volume was equal to that of the nondisplaceable compartment in the basal ganglia. Both methods yielded a similar estimation of BP. Thus [^{123}I]IBF satisfies the condition of reversibility needed for implementation of this graphic method, which is computationally simpler and faster than the kinetic modeling approach.

K_1 and k_2 were well identified by kinetic modeling and relatively stable across subjects. Using Equation 8 and an average basal ganglial blood flow of 0.65 ml · g^{-1} · min^{-1} (*33*), the mean basal ganglial K_1 estimates E as 0.18, PS as 0.13 ml · g^{-1} · min^{-1} and the PS product relative to the free compound (PS/f_1; *17,34*) at 2.72 ml · g^{-1} · min^{-1}. Thus, the relatively low extraction is compatible with the high level of binding to plasma proteins measured in vitro. Occipital K_1 values were lower than striatal K_1 values, reflecting the lower blood flow in white matter compared with that in gray matter and the larger white matter contribution to the occipital ROI compared with that in the basal ganglia.

Individual values of k_3 and k_4 exhibited high covariance, but their ratio was well identified by the regression. As previously described (*18,20*), the identifiability of k_3 and k_4 values increases as k_4 became much lower than k_2. When k_4 is equal to or greater than k_2, the eigenvalue of the second exponential of the impulse response function becomes relatively insensitive to k_4 if the k_3-to-k_4 ratio was fixed.

Basal ganglial peak uptake occurred later in humans (52 ± 24 min) than in baboons (20–40 min, *15*). This difference appeared related to the slower peripheral clearance in humans (0.63 ± 0.38 liter/hr · kg) compared with that in baboons (1.42 ± 0.66 liter/hr · kg, n = 10, unpublished data). The mean value of k_4 in human was 0.035 ± 0.020 min^{-1}, corresponding to a dissociation half-life of 19 ± 11 min. This value compares favorably with the [^{123}I]IBF dissociation half-life measured in baboons (28 ± 18 min, n = 3) with a similar constrained three-compartment model (unpublished data). In baboons, [^{123}I]IBF in vivo equilibrium binding was decreased by drugs such as dextroamphetamine, which increase dopamine intrasynaptic concentrations (*16*). Because the in vivo k_{off} appears to be the critical factor determining the sensitivity of a tracer to this type of challenge (*35*), these data suggest that such a paradigm might be implemented in humans with [^{123}I]IBF to study dextroamphetamine-induced dopamine release.

Three outcome measures were proposed to characterize the equilibrium distribution volume of the receptor compartment. The first outcome measure, V_3, is theoretically equivalent to the molecular binding potential. Combining experiments performed at high and low specific activity, the authors recently measured the in vivo [^{123}I]IBF K_D in baboons as 0.09 n*M* (unpublished results), a value in close agreement with the in vitro [^{125}I]IBF K_D measured at 37°C (0.11 n*M*, *7*). Assuming a similar in vivo K_D in humans, a BP of 129 ± 51 would correspond to a B_{max} of 11.6 ± 4.6 n*M*.

This in vivo [^{123}I]IBF B_{max} value is in excellent agreement with the in vitro D2 B_{max} value of 11.5 ± 3.6 n*M*, as measured with [^{3}H]spiperone in postmortem human basal ganglia samples (n = 246, age range 43–93 yr, *36*). However, this comparison may be misleading for two reasons. First, the D2 B_{max} for benzamides such as [^{3}H]emonapride or [^{3}H]raclopride was shown to be 1.5- to 2-fold higher than the D2 B_{max} for [^{3}H]spiperone in D2 cloned cell lines (*37*), and a D2 B_{max} value of 16.5 ± 4.7 n*M* in human postmortem caudate samples was recently reported for the benzamide [^{125}I]epidipride (n = 6, age range 65–89 yr, *38*). Second, postmortem and PET studies show a decline in D2 receptor density with age (*39–44*). PET experiments performed with [^{11}C]raclopride in subjects between their sec-

TABLE 4
Basal Ganglia: Kinetic and Graphic Analyses*

	Kinetic analysis							Graphic analysis					
Study no.	K_1 (ml g^{-1} min^{-1})	k_2 (min^{-1})	k_3 (min^{-1})	k_4 (min^{-1})	V_3 (ml/g)	V'_3 (ml/g)	V''_3 (ml/g)	k_3 (min^{-1})	k_4 (min^{-1})	V_3 (ml/g)	V'_3 (ml/g)	V''_3 (ml/g)	Difference (%)
1	0.170	0.0550	0.0742	0.0298	110	7.73	2.49	0.0348	0.0144	109	7.65	2.42	1.0
2	0.143	0.0550	0.0937	0.0280	181	8.66	3.35	0.0624	0.0180	188	9.01	3.46	4.0
3	0.165	0.0548	0.0740	0.0298	139	7.49	2.48	0.0188	0.0073	132	7.14	2.58	4.7
4	0.122	0.0499	0.1940	0.0833	88	5.71	2.33	0.0321	0.0137	88	5.71	2.34	0.0
5	0.087	0.0400	0.0302	0.0196	139	3.34	1.54	0.0820	0.0678	116	2.78	1.21	16.6
6	0.093	0.0509	0.1060	0.0429	70	4.50	2.46	0.0979	0.0378	70	4.50	2.59	0.0
7	0.112	0.0408	0.0425	0.0246	103	4.74	1.73	0.2726	0.1726	97	4.45	1.58	6.1
8	0.090	0.0551	0.0883	0.0238	226	6.09	3.72	0.0679	0.0186	222	6.01	3.65	1.4
Mean	0.123	0.0502	0.0878	0.0352	132	6.03	2.51	0.0836	0.0438	128	5.91	2.48	4.24
± s.d.	0.033	0.0064	0.0499	0.0206	51	1.83	0.73	0.0809	0.0556	52	2.00	0.83	5.51

*Difference between two methods was calculated as the absolute value of the difference between kinetic V_3 and graphical V_3, expressed as percentage of kinetic V_3.

K_1 and k_2 = fractional rate constants of the tracer transport in and out of the brain; k_3 and k_4 = tracer-receptor association and dissociation rate constants; V_3 = equilibrium distribution volume of receptor compartment relative to free tracer in arterial plasma, equal to binding potential; V'_3 = equilibrium distribution volume of receptor compartment relative to total tracer in arterial plasma; V''_3 = equilibrium distribution volume of receptor compartment relative to occipital equilibrium distribution volume, equal to k_3/k_4.

ond and fourth decades provided B_{max} estimates of 14.4 ± 1.9 n*M* (*45*), 22 ± 6 n*M* (*46*) and 25 to 45 n*M* (*43*). Thus, [^{123}I]IBF B_{max}, as measured here, may be underestimated, presumably because of the partial volume effects associated with the use of a relatively large ROI.

The large range of V_3 estimated by this study (70–226 ml/g) is in accordance with the range of D2 densities reported in PET studies in this age group: 5 to 30 n*M* (*47*), 15 to 40 n*M* (*46*) and 25 to 45 n*M* (*43*). However, between-subject variations in BP were strongly influenced by variations in f_1. This observation raised concerns about error propagation from the f_1 measurement to the final outcome measure. Because only a small fraction (about 5%) of [^{123}I]IBF is not bound to plasma proteins, small differences between subjects in the percent free have a significant impact on the calculation of V_3. Under these conditions, the equilibrium distribution volume relative to the total plasma tracer (V'_3) might be a better outcome measure. Indeed, the majority of PET studies looking at measurements of D2 receptor density neglected potential f_1 differences between subjects (*17,43,45,48,49*). It should, however, be noticed that this question is only of concern when BP is chosen as the outcome measure. When B_{max} and K_D are derived with paired high and low specific activity experiments, differences in f_1 affect the K_D but not the B_{max}.

TABLE 5
Basal Ganglia: Kinetic and Empiric Analyses*

Study no.	Kinetic analysis V''_3 (ml/g)	Empiric method (specific-to-nonspecific ratio from 80–120 min)	Difference (%)
1	2.49	2.33	7
2	3.35	2.90	13
3	2.48	2.38	4
4	2.33	2.52	8
5	1.54	1.46	5
6	2.46	2.38	3
7	1.73	1.64	5
8	3.72	2.53	32
Mean ± s.d.	2.51 ± 0.73	2.27 ± 0.48	10 ± 10

*Difference between the two methods was calculated as the absolute value of the difference between the outcome measures, expressed as percentage of V''_3.

V''_3 = equilibrium distribution volume of receptor compartment relative to occipital equilibrium distribution volume, calculated as k_3/k_4; specific-to-nonspecific ratio = ratio of basal ganglial minus occipital counts to occipital counts, averaged for four acquisitions between 80 and 120 min.

An alternative solution is to express the outcome measure in terms of BP/V_2 (= k_3-to-k_4 ratio or = V''_3). This outcome measure, also designed as the equilibrium partition coefficient (*50*), presents several advantages. Because f_1 is included in both the numerator and denominator, this ratio is independent of f_1 and protected both from potential experimental errors and between-subject variations in f_1 that may bias the measurement. In addition, V''_3 is protected from potential errors in the cross calibration between the brain and plasma counting devices. The underlying assumption is the uniformity of the nondisplaceable compartment across subjects. This assumption appears to be reasonable because V'_2 showed the lowest between-subject variation of all the calculated outcome measures. It is likely that the protection from experimental errors associated with the choice of V''_3 as the outcome measure exceeds the error introduced by the assumption of between-subject uniformity of V_2. Assessment of between-experiment reproducibility for each outcome measure with a test/retest paradigm is needed to address this issue further and ultimately to select the method most sensitive to alterations in D2 BP (*49,51*).

An analytic method that does not require repeated scan acquisitions and plasma measurements significantly decreases the cost of the studies and increases patient compliance. In theory, V_3'' could be directly estimated from the specific-to-nonspecific ratio at the peak time of the specific binding. A 40-min time interval (80–120 min), centered around the average specific binding peak time, was thus chosen as the period during which the specific-to-nonspecific ratio was most likely to be in agreement with V_3''. The average difference between this ratio and V_3'' was 10%, and most of the difference was caused by two subjects who combined slow clearance and high BP. The use of a later time interval in these two subjects would have reduced this error. These data, and the simulations performed with the kinetic parameters derived from the present study, illustrated the potential error associated with the use of a predefined and limited scanning interval. Whether or not this 10% error is acceptable for clinical investigations depends on multiple factors, such as the expected magnitude of the D2 density alteration and the number of subjects. Thus, this question should be addressed by a power analysis prior to such an investigation.

The error associated with the empiric ratio method ultimately derives from the fact that the basal ganglia-to-oc-

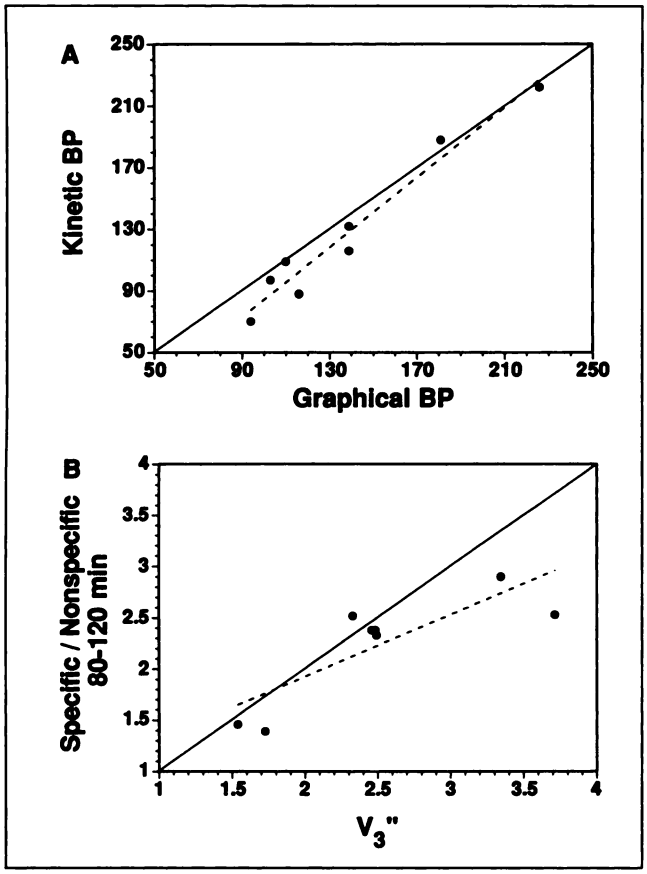

FIGURE 6. Relationship between kinetically, graphically and empirically derived outcome measures. The solid line represent the ideal situation in which the outcome measures would be linearly related with a slope of one. The broken line represents the linear regression of the measured values. (A) The relationship between the graphic BP and the kinetic BP was linear with a slope of 1.13 (r^2 = 0.94, p = 0.0001). (B) The relationship between the empiric specific-to-nonspecific ratio averaged from 80 to 120 min and the kinetic V_3'' was linear (p = 0.01) but had a slope of 0.060 and a r^2 of 0.68. The two points in the upper right were affected by the highest residuals and corresponded to Subjects 2 and 8 who combined slow clearance (Table 2) and high BP (Table 4). In these subjects, specific binding equilibration (time of peak specific uptake) occurred after 120 min.

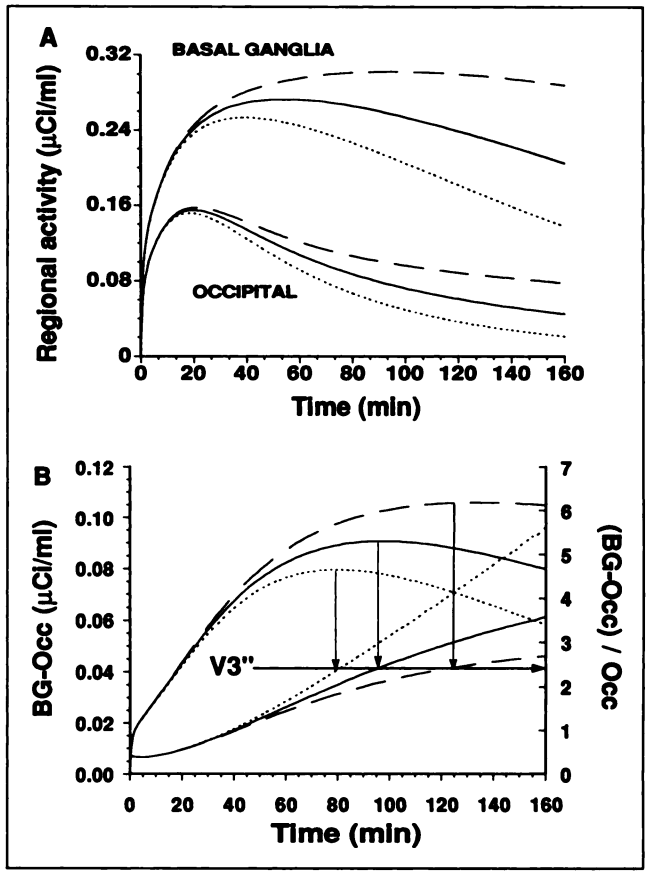

FIGURE 7. Simulated curves to investigate effect of peripheral clearance on empirically measured distribution volume. (A) Basal ganglial and occipital time-activity curves were obtained by convoluting occipital and basal ganglial average impulse response functions (see parameter values in text) by three input functions. These input functions were characterized by control peripheral clearance (equal to population sample mean value, 41 liters/hr, solid lines), fast clearance (63 liters/hr, dotted lines) and slow clearance (19 liters/hr, broken lines). As plasma clearance becomes slower, the regional peak uptake time is delayed, and the regional washout rate decreases. (B) Empiric analysis. Specific binding (left y-axis, three upper curves) was measured as the difference between basal ganglial (BG) and occipital (Occ) activities and plotted as a function of time for the control, fast and slow clearance situations. Specific-to-nonspecific ratios were then calculated for each time (right y-axis, three lower curves). At specific binding peak time (79, 96 and 120 min in fast, control and slow plasma clearance simulations, respectively), the specific-to-nonspecific ratio was equal to 2.49 (= true value of V_3'' used in the impulse response function parameters). Hence, an empiric outcome measured based on this ratio between 80 and 120 min would overestimate the true V_3'' in case of a fast clearance and underestimate the true V_3'' in case of a slow clearance.

cipital ratio is only linear with the receptor density at equilibrium, i.e., at the peak time of the specific binding. After a single bolus injection, this equilibrium state is only established for a short time. As previously described with [^{11}C]cyclofoxy (*52*) and [^{123}I]iomazenil (*53*), this difficulty can be circumvented by the administration of the tracer as a constant infusion. During a tracer constant infusion, a prolonged state of equilibrium can be established and maintained for a prolonged period (*52,53*). Preliminary studies in baboons suggested that a constant infusion paradigm could be implemented for [^{123}I]IBF (*16*), and the feasibility of this approach in humans is currently under investigation.

The average equilibrium specific-to-nonspecific ratio measured in this study was 2.51 ± 0.75. This value is four- to fivefold higher than the corresponding values reported for [^{123}I]IBZM in humans, ranging from 0.5 to 0.75 (*54,55*). Thus, in accordance with previous reports in rodents (*7,10,56*), [^{123}I]IBF has a higher target-to-background ratio than does [^{123}I]IBZM in humans.

Studies based on one high specific activity injection are limited to the derivation of BP and do not provide explicit derivations of B_{max} and K_D. Paired high and low specific activity injections are required to measure these parameters. Toxicologic studies are needed to evaluate the safety of injection of pharmacologic doses of IBF before implementing [^{123}I]IBF low specific activity injections in humans. The potential sensitivity of the BP to the endogenous dopamine level is one limitation of the use of BP as an outcome measure. However, the explicit derivation of B_{max} and K_D might not be sufficient to protect the D2 measurement from the effects of endogenous dopamine. Because of the existence of high and low affinity states of the D2 receptors, the interaction between dopamine and dopamine antagonists is pseudononcompetitive (*57*), which means that dopamine affects both the apparent B_{max} and K_D of the antagonists (*58–60*).

In conclusion, [^{123}I]IBF provided high basal ganglial-to-occipital ratios and good reversibility. Both of these qualities are needed for quantitative measurement of D2 BP with SPECT in humans. Kinetic and graphic analyses could be implemented and yielded identical results. Several outcome measures were proposed, and test/retest studies are needed to define their reproducibility.

ACKNOWLEDGMENTS

The authors thank E. O. Smith, G. Wisniewski, L. Pantages-Torok, MD Stratton and Q. Ramsby for excellent technical assistance. This work was supported in part by funds from the Department of Veterans Affairs (Schizophrenia Research Center and the Center for the Study of Post-traumatic Stress Disorder) and the Public Health Service (MH25642 and MH30929).

REFERENCES

1. Kung HF, Pan S, Kung M-P, et al. In vitro and in vivo evaluation of [^{123}I]IBZM: a potential CNS D-2 dopamine receptor imaging agent. *J Nucl Med* 1989;30:88–92.
2. Pedro BM, Gray NS, Pilowsky LS, et al. Dopamine D2 receptor binding in the basal ganglia in schizophrenia: relationship to stereotypy. *Schizophr Res* 1993;9:186.
3. Tatsch K, Schwarz J, Oertel WH, Kirsh CM. Dopamine D2 receptor imaging with I-123 IBZM SPECT to differentiate idiopathic from other Parkinson syndromes [Abstract]. *J Nucl Med* 1992;33:917.
4. Brucke T, Podreka I, Angelberger P, et al. Dopamine D2 receptor imaging with SPECT: studies in different neuropsychiatric disorders. *J Cereb Blood Flow Metab* 1991;11:220–228.
5. Laulumaa V, Kuikka JT, Soininen H, et al. Imaging of D2 dopamine receptor of patients with Parkinson's disease using single photon emission computed tomography and iodobenzamide I-123. *Ann Neurol* 1993;50:509–512.
6. van Royen E, Verhoeff NFLG, Speelman JD, et al. Multiple system atrophy and progressive supranuclear palsy. Diminished striatal D2 receptor activity demonstrated by ^{123}I-IBZM single photon emission computed tomography. *Ann Neurol* 1993;50:513–516.
7. Kung M-P, Kung HF, Billings J, et al. The characterization of IBF as a new selective dopamine D-2 receptor imaging agent. *J Nucl Med* 1990;31:648–654.
8. Hall H, Hogberg T, Halldin C, et al. NCQ 298, a new selective iodinated salicylamide ligand for the labeling of dopamine D2 receptors. *Psychopharmacology* 1991;103:6–18.
9. Kessler RM, Ansari MS, Schmidt DE, et al. High affinity dopamine D2 receptor radioligands. 2. [^{125}I]Epidepride, a potent and specific radioligand for the characterization of striatal and extrastriatal dopamine D2 receptors. *Life Sci* 1991;49:617–628.
10. Kessler RM, Ansari MS, de Paulis T, et al. High affinity dopamine D2 receptor radioligands. 1. Regional rat brain distribution of iodinated benzamides. *J Nucl Med* 1991;32:1593–1600.
11. Carson RE. Precision and accuracy considerations of physiological quantification in PET. *J Cereb Blood Flow Metab* 1991;11:A45–A50.
12. Carson RE. The development and application of mathematical models in nuclear medicine. *J Nucl Med* 1991;32:2206–2208.
13. Gjedde A, Wong DF. Modeling neuroreceptor binding of radioligands in vivo. In: Frost JJ, Wagner HN Jr, eds., *Quantitative imaging: neuroreceptors, neurotransmitters, and enzymes*. New York: Raven Press; 1990:51–79.
14. Mintun MA, Raichle ME, Kilbourn MR, Wooten GF, Welch MJ. A quantitative model for the in vivo assessment of drug binding sites with positron emission tomography. *Ann Neurol* 1984;15:217–227.
15. Al-Tikriti MS, Baldwin RB, Zea-Ponce Y, et al. Comparison of three high affinity SPECT radiotracers for the dopamine D2 receptors. *Nucl Med Biol* 1994;21:179–188.
16. Laruelle M, Al-Tikriti M, van Dyck CH, et al. D-amphetamine displacement of [^{123}I]IBF equilibrium binding in primates: a new paradigm to investigate D-amphetamine induced dopamine release. *Schizophr Res* 1993;9:201.
17. Logan J, Wolf AP, Shiue CY, Fowler JS. Kinetic modeling of receptor-ligand binding applied to positron emission tomographic studies with neuroleptic tracers. *J Neurochem* 1987;48:73–83.
18. Frost JJ, Douglass KH, Mayberg HS, et al. Multicompartmental analysis of ^{11}C-carfentanil binding to opiate receptors in human measured by positron emission tomography. *J Cereb Blood Flow Metab* 1989;9:398–409.
19. Koeppe RA, Holthoff VA, Frey KA, Kilbourn MR, Kuhl DE. Compartmental analysis of [^{11}C]flumazenil kinetics for the estimation of ligand transport rate and receptor distribution using positron emission tomography. *J Cereb Blood Flow Metab* 1991;11:735–744.
20. Logan J, Fowler J, Volkow ND, et al. Graphical analysis of reversible radioligand binding from time-activity measurements applied to [N-^{11}C-methyl]-(-)-cocaine PET studies in human subjects. *J Cereb Blood Flow Metab* 1990;10:740–747.
21. Murphy RA, Kung HF, Kung M-P, Billings J. Synthesis and characterization of iodobenzamide analogs: potential D-2 dopamine receptor imaging agents. *J Med Chem* 1990;33:171–178.
22. United States Pharmacopeial Convention, Inc. *The United States Pharmacopeia*, 22nd revision. Rockville, MD: United States Pharmacopeial Convention; 1990.
23. Holman BL, Carvalho PA, Zimmerman RE, et al. Brain perfusion SPECT using an annular single crystal camera: initial clinical experience. *J Nucl Med* 1990;31:1456–1461.
24. Zubal IG, Harrell C, Woods SW, et al. Comparison of quantitation linearity of three brain SPECT imaging instruments using Tc-99m and I-123. *J Nucl Med* 1990;31:769–770.
25. Zoghbi SS, Baldwin RM, Seibyl JP, et al. Pharmacokinetics of the SPECT benzodiazepine receptor radioligand [^{123}I]iomazenil in human and nonhuman primates. *Nucl Med Biol* 1992;19:881–888.

26. Lidow MS, Goldman-Rakic PS, Rakic P, Innis RB. Dopamine D2 receptors in the cerebral cortex: distribution and pharmacological characterization with [^{3}H]raclopride. *Proc Natl Acad Sci USA* 1989;86:6412–6416.
27. Laruelle M, Baldwin RM, Rattner Z, et al. SPECT quantification of [^{123}I]iomazenil binding to benzodiazepine receptors in nonhuman primates. I. Kinetic modeling of single bolus experiments. *J Cereb Blood Flow Metab* 1994;14:439–452.
28. Phelps ME, Huang SC, Hoffman EJ, et al. Tomographic measurement of local cerebral glucose metabolic rate in humans with (F-18)2-fluoro-2-deoxy-D-glucose: validation of method. *Ann Neurol* 1979;6:371–382.
29. Frey KA, Hichwa RD, Ehrenkaufer RLE, Agranoff BW. Quantitative in vivo receptor binding III: tracer kinetic modeling of muscarinic cholinergic receptor binding. *Proc Natl Acad Sci USA* 1987;82:6711–6715.
30. Levenberg K. A method for the solution of certain problems in least squares. *Q Appl Math* 1944;2:164–168.
31. Carson RE. Parameters estimation in positron emission tomography. In: Phelps ME, Mazziotta JC, and Schelbert HR, eds., *Positron emission tomography. Principles and applications for the brain and the heart*. New York: Raven Press; 1986:347–390.
32. Dittmer DS. *Blood and other body fluids*. Washington, DC: Federation of American Societies for Experimental Biology; 1961.
33. Mazziotta JC, Phelps ME. Positron emission tomography studies of the brain. In: Phelps ME, Mazziotta JC, and Schelbert HR, eds., *Positron emission tomography. Principles and applications for the brain and the heart*. New York: Raven Press; 1986:493–579.
34. Sawada Y, Hiraga S, Patlak CS, et al. Cerebrovascular transport of [^{125}I]quinuclidinyl benzilate, [^{3}H]cyclofoxy, and [^{14}C]iodoantipyrine. *Am J Physiol* 1990;258:H1585–H1598.
35. Kessler RM, Mason NS, Votaw JR, et al. Factors underlying the D-amphetamine induced displacement of dopamine D2 radioligands in rhesus monkeys [Abstract]. *J Nucl Med* 1993;34:132P.
36. Seeman P, Bzowej NH, Guan HC, et al. Human brain D1 and D2 dopamine receptors in schizophrenia, Alzheimer's, Parkinson's, and Huntington's diseases. *Neuropsychopharmacology* 1987;1:5–15.
37. Seeman P, Guan HC, Civelli O, et al. The cloned dopamine D2 receptor reveals different densities for dopamine receptor antagonist ligands. Implications for human brain positron emission tomography. *Eur J Pharmacol* 1992;227:139–146.
38. Kessler RM, Whetsell WO, Ansari MS, et al. Identification of extrastriatal dopamine D2 receptors in postmortem human brain with [^{125}I]epidipride. *Brain Res* 1993;609:237–343.
39. Rinne JO. Brain muscarinic and dopaminergic receptors in the aging human brain. *Brain Res* 1987;404:162–168.
40. Seeman P, Bzowej NH, Guan HG, et al. Human brain dopamine receptors in children and aging adults. *Synapse* 1987;1:399–404.
41. Rinne JO, Lönnberg P, Marjamäki P. Age-dependent decline in human brain D-1 and D-2 receptors. *Brain Res* 1990;508:349–352.
42. Wong DF, Wagner HN, Dannals RF, et al. Effects of age on dopamine and serotonin receptors measured by positron emission tomography in the lining brain. *Science* 1984;226:1393–1396.
43. Rinne JO, Hietala J, Ruotsalainen U, et al. Decrease in human striatal dopamine D2 receptor density with age: a PET study with [^{11}C]raclopride. *J Cereb Blood Flow Metab* 1993;13:310–314.
44. Antonini A, Leenders KL, Reist H, et al. Effect of age on D2 dopamine receptors in normal human brain measured by positron emission tomography and ^{11}C-raclopride. *Ann Neurol* 1993;50:474–480.
45. Farde L, Hall H, Ehrin E, Sedvall G. Quantitative analysis of D2 dopamine receptor binding in the living human brain by PET. *Science* 1986;231:258–261.
46. Farde L, Wiesel F, Stone-Elander S, et al. D2 dopamine receptors in neuroleptic-naive schizophrenic patients. A positron emission tomography study with [^{11}C]raclopride. *Arch Gen Psychiatry* 1990;47:213–219.
47. Wong DF, Wagner HNJ, Tune LE, et al. Positron emission tomography reveals elevated D2 dopamine receptors in drug-naive schizophrenics. *Science* 1986;234:1558–1563.
48. Wong DF, Gjedde A, Wagner HNJ, et al. Quantification of neuroreceptors in the living brain. II. Inhibition studies of receptor density and affinity. *J Cereb Blood Flow Metab* 1986;6:147–153.
49. Volkow ND, Fowler JS, Wang GJ, et al. Reproducibility of repeated measures of carbon-11-raclopride binding in the human brain. *J Nucl Med* 1993;34:609–613.
50. Salmon E, Brooks DJ, Leenders KL, et al. A two compartment description and kinetic procedure for measuring regional cerebral [^{11}C]nomifensine uptake using positron emission tomography. *J Cereb Blood Flow Metab* 1990;10:307–316.
51. Vingerhoets FJG, Snow BJ, Schulzer M, et al. Reproducibility of fluorine-18-fluorodopa positron emission tomography in normal human subjects. *J Nucl Med* 1994;35:18–24.
52. Carson RE, Channing MA, Blasberg RG, et al. Comparison of bolus and infusion methods for receptor quantification: application to [^{18}F]-cyclofoxy and positron emission tomography. *J Cereb Blood Flow Metab* 1992;13:24–42.
53. Laruelle M, Abi-Dargham A, Al-Tikriti MS, et al. SPECT quantification of [^{123}I]iomazenil binding to benzodiazepine receptors in nonhuman primates. II. Equilibrium analysis of constant infusion experiments and correlation with in vitro parameters. *J Cereb Blood Flow Metab* 1994;14:453–465.
54. Seibyl J, Woods S, Zoghbi S, et al. Dynamic SPECT imaging of D2 receptors in human subjects with iodine-123-IBZM. *J Nucl Med* 1992;33:1964–1971.
55. Kung HF, Alavi A, Chang W, et al. In vivo SPECT imaging of CNS D-2 dopamine receptors: initial studies with iodine-123 IBZM in humans. *J Nucl Med* 1990;31:573–579.
56. Kung HF, Guo Y-Z, Billings J, et al. Preparation and biodistribution of [^{125}I]IBZM: a potential CNS D-2 dopamine receptor imaging agent. *Nucl Med Biol* 1988;15:195–201.
57. Sibley DR, Creese I. Pseudo non-competitive interactions with dopamine receptors. *Eur J Pharmacol* 1980;65:131–133.
58. Sibley DR, De Lean A, Creese I. Anterior pituitary receptors: demonstration of interconvertible high and low affinity states of the D2 dopamine receptor. *J Biol Chem* 1982;257:6351–6361.
59. Seeman P, Niznik HB, Guan H-C. Elevation of dopamine D2 receptors in schizophrenia is underestimated by radioactive raclopride. *Arch Gen Psychiatry* 1990;47:1170–1172.
60. Hall H, Wedel I, Halldin CJK, Farde L. Comparison of the in vitro binding properties of N-[^{3}H]methylspiperone and [^{3}H]raclopride to rat and human brain membranes. *J Neurochem* 1990;55:2048–2057.